Cite this: DOI: 10.1039/c0xx00000x

www.rsc.org/xxxxxx

ARTICLE TYPE

Evidence of Structural Variability among Synthetic and Biogenic Vaterite

Giuseppe Falini[a,*], Simona Fermani[a], Michela Reggi[a], Branka Njegić Džakula[b] and Damir Kralj[b]

Received (in XXX, XXX) Xth XXXXXXXXX 20XX, Accepted Xth XXXXXXXXX 20XX

DOI: 10.1039/b000000x

Recently, the results of experimental and theoretical investigations have revealed that, in vaterite, two or even more crystalline structures coexist. In this communication we report evidence of diverse vaterite structures in biogenic samples of different origin. In addition, it is shown that the synthetic vaterite precipitated in the presence of poly-L-aspartate, holds structures similar to those of biogenic samples.

Calcium carbonates occur widely in nature, having an important role in many biological functions and processes in living organisms.[1,2,3] In addition, they are the major minerals in many sedimentological environments. Calcium carbonates are also valuable in many industrial applications, such as paper, rubber, plastics, and paint production.[4,5,6,7]

At ambient conditions of temperature and pressure, calcium carbonates appear in the form of three polymorphs and several hydrated phases. Of these, vaterite is thermodynamically unstable with respect to the other anhydrous crystalline polymorphs, aragonite and calcite, which explains its rare appearance as a mineral in geological settings. At the same time, during the early stages of conventional precipitation systems, vaterite formation was observed and explained by Ostwald's rule of stages.[8] It postulated the initial formation of a thermodynamically less stable (more soluble) modification, in a system supersaturated with respect to several solid phases, and its subsequent transformation into a stable phase. On the other hand, vaterite is stable with respect to hydrated modifications and amorphous calcium carbonates (ACCs),[9] so it plays an important role as a precursor in several carbonate-forming processes.[10] However, the natural occurrence of vaterite is usually associated with biogenic activities. In the case of pathological mineralization, vaterite appears in pancreatic and gallstone formation or clogging in human heart valves.[11] As a biomineral, vaterite is present in fish otoliths,[12,13] crustacean statoliths,[14] green turtle eggshells,[15] freshwater lackluster pearls,[16] aberrant growth of mollusk shells after an injury,[17] or spicules of the ascidian *Herdmania momus*.[18]

Preparation of synthetic vaterite has been extensively investigated and described, either in the precipitation systems without the addition of the additive,[19] or at additive assisted[20] or template-directed[21,22] conditions.

One of the most striking features of vaterite is the wide variety of shapes and morphologies it can hold,[10] which is related to its high surface energy.[23] On the other hand, researchers not yet succeeded in producing single crystals of vaterite of suitable quality for an accurate structure determination by X-ray diffraction. Consequently, the crystal structure of vaterite has been controversial and not well understood. Only recently, Kabalah-Amitai *et al.*,[24] used high-resolution, aberration-corrected transmission electron microscope (HR-TEM) and found that in a "single crystal" of vaterite, isolated from the biogenic spicules of *H. momus*, a predominantly hexagonal structure coexists with one, or even more, distinct crystallographic structures.

At the same time, Demichelis *et al.*[25] proposed theoretically the existence of several stable vaterite structures, which required just room-temperature thermal energy for their inter-conversions. The authors also concluded that the vaterite is not a single "disordered" structure, but it should be considered as a combination of different forms. The possible presence of biological molecules was not considered in the described studies and their potential effect on the structure inter-conversions was not discussed, in spite of the fact that biological macromolecules have a demonstrated role in the stabilization of vaterite. Specifically, it was observed that the biogenic vaterite is stable in water solution for months, while under similar conditions, synthetic samples rapidly convert to calcite.[24,26] Consequently, the possibility that the control of the distribution of vaterite structures is species specific and caused by particular macromolecules cannot be excluded.

Although recent studies contributed to the understanding of the vaterite structure[24,25] and explained discrepancies among experimental and theoretical data, the question of the role of organisms in the formation of species specific vaterite structures remained open.

In this study the structural features of synthetic and biogenic vaterite samples were compared (Fig. 1). More specifically, the biogenic vaterite samples were isolated from the asteriscus otolith from the *Condrostoma nasus*, the Chinese freshwater cultured lackluster pearl (from *Hyriopsis Cumingii* mussels) and the spicule of the ascidian *H. momus*. Synthetic vaterite samples were precipitated by mixing solutions of $CaCl_2$ and Na_2CO_3/ $NaHCO_3$ at lower initial concentrations, $c_i(Ca)$ = $c_i(CO_3)$ = 1.0 mM (vat1), and at higher initial concentrations, $c_i(Ca)$ = $c_i(CO_3)$ = 2.5 mM (vat2). In the system of higher concentrations, the supersaturation was, S_{vat} = 6.36, while in the lower concentration system, $S_{vat} = 3.71$.[19,20]

Synthetic vaterite samples were also prepared in the presence of poly-L-aspartate (pAsp) dissolved in the carbonate solution, applying a similar protocol and keeping the Ca^{2+}/pAsp molar ratio constant. The pAsp concentrations, c = 1.25 ppm (vat1-pAsp) or c = 3.00 ppm (vat2-pAsp), were used in the 1.0 mM or 2.5 mM systems, respectively. This polypeptide was used as a synthetic analogue of the intra-skeletal acidic macromolecules of biogenic vaterite.[12]

The X-ray diffraction analyses showed the presence of vaterite as a unique crystalline phase in all biogenic samples while, in the synthetic samples, traces of calcite were detected (Fig. S1).

The differences between the particle shapes and morphologies of synthetic and biogenic vaterite were significant, as shown in Fig. 1.

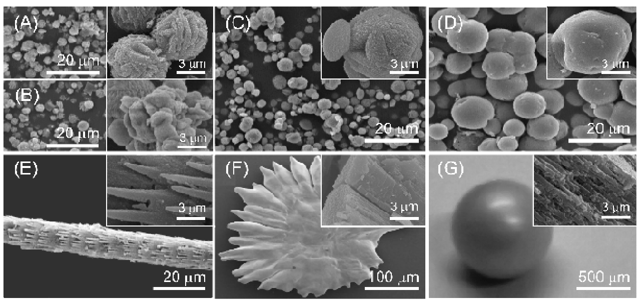

Fig. 1 Scanning electron microscope pictures of: (A) vat1; (B) vat2; (C) vat1-pAsp; (D) vat2-pAsp; (E) *H. momus* spicule; (F) *C. nasus* asteriscus otolith; (G) lackluster pearl.

The synthetic vaterite appeared predominantly as spherical structures, built up of hexagonal plate-like aggregates. The shape and morphology of the vat1-pAsp particles were similar to those of pure synthetic vaterite, while the surfaces of the vat2-pAsp particles appeared much smoother. The shapes of the biogenic vaterite samples, as well as the respective primary building blocks, were found to be species specific. The ascidian spicule was built up from acicular prisms, asteriscus otolith from prisms and the primary building blocks of lackluster pearl were tablets.

The initial indication of structural diversities among the samples was gained by the grinding curves (Fig. 2). The curves were obtained by repeated grinding of the sample and plotting the intensity of the ν_2 band (normalized with respect to ν_3 band) against the normalized ν_4 band, after each grinding. For each sample, a curve with a well-defined trend line was obtained. The offsets between curves reflected the differences in short range atomic disorder.[27,28] The results indicated that the grinding curves obtained for biogenic vaterite samples were localized in the same region of the graph, thus pointing to a similar atomic order. The samples of pure synthetic vaterite showed curves localized far from the biogenic ones. However, the curves of synthetic vat1-pAsp and vat2-pAsp samples were localized in the graph region between the curves of the pure synthetic and the biogenic vaterite, with the latter closer to the biogenic and the former to the pure synthetic ones.

The different number of peaks in the ν_3 band of the FTIR spectra of vaterite samples offered additional information on their structure[29] (Fig. 3). The synthetic vaterite samples showed a central peak at 1465 cm^{-1} and two weaker side peaks at 1492 and 1437 cm^{-1}. In *H. momus* spicule the peak at 1492 cm^{-1} was the most intense and an additional peak appeared at 1408 cm^{-1}. In *C. nasus* asteriscus, the most intense vibration was that at 1437 cm^{-1}, while in lackluster pearl those at 1492 and 1465 cm^{-1} were the most intense. Diverse profiles were also observed in Raman spectra, where the symmetric stretching vibration (ν_1) of carbonates revealed a triplet in some studies and a doublet in others.[13] The split in the degenerate ν_3 carbonate stretching mode results from the modification of the electrostatic environment of the Ca–O bond.[30] Thus, the observed source specific profile of the ν_3 band in the vaterite samples is in agreement with a possible co-existence of diverse crystalline structures,[24,25] which depend on various Ca^{2+} coordination geometries. However, these vibrations could not be assigned to specific structural domains in vaterite samples.

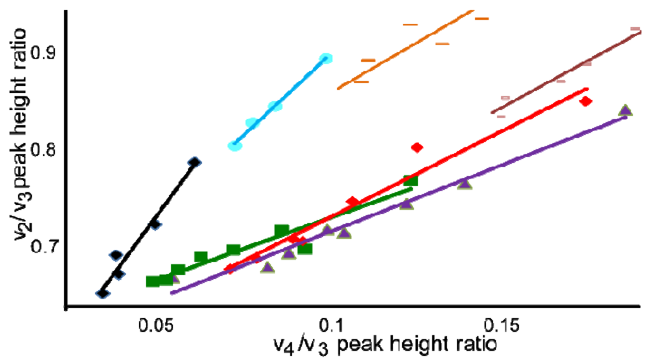

Fig. 2 Grinding curves of vaterite samples. (♦) vat1; (●) vat2; (–) vat1-pAsp; (–) vat2-pAsp; (■) *H. momus* spicule; (▲) *C. nasus* asteriscus; (♦) lackluster pearl.

The ν_3 band appeared to be more structured in the biogenic samples than in the synthetic ones. In addition, it could be observed that the ν_3 band of the vat2-pAsp was more structured than for the other synthetic vaterites.

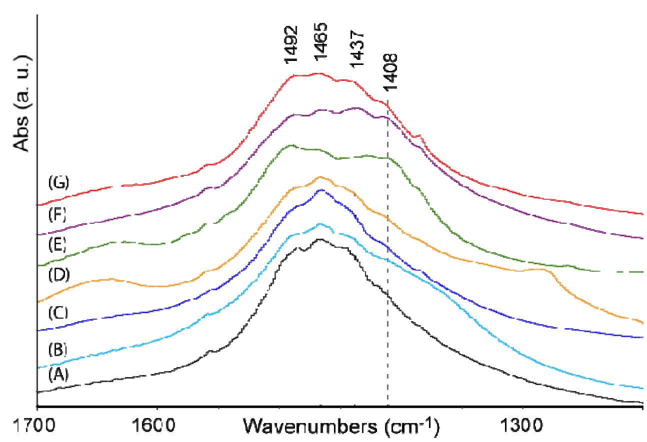

Fig. 3 FTIR spectrum in the range of ν_3 band of: (A) vat1; (B) vat2; (C) vat1-pAsp; (D) vat2-pAsp; (E) *H. momus* spicule; (F) *C. nasus* asteriscus; (G) lackluster pearl. The full spectra in the range 4000-500 cm^{-1} are reported in Fig. S2.

In Fig. 4 the differential scanning calorimetry (DSC) profiles of vaterite samples were shown, while the results of their analysis are summarized in Table S1. It can be seen that only the samples of pure synthetic vaterite showed a sharp endothermic band centred at 477 °C, while the other vaterite samples showed broader endothermic bands. The maximum of vat1-pAsp profile is at 465 °C with a shoulder at 477 °C, while the vat2-pAsp profile's maximum is at 463 °C and has a broad shoulder at about 419 °C. Vaterite from spicules and otoliths showed endothermic band maxima at 420 °C and at 431 °C, respectively. The vaterite isolated from pearl showed a band with the maximum at about 533 °C, in agreement with the reported data.[31] In all samples vaterite converted completely to calcite after the thermal treatment, at temperatures corresponding to maximum of the reported endothermic bands (Fig. S3). Therefore, these temperatures represented the temperature of vaterite to calcite transition. The observed different metastability of the vaterite samples has been supposed to be caused by the co-presence of the organic matrix, polypeptides, foreign ions and/or water molecules.[32] Nevertheless, it the possibility that the different co-existing crystalline structures contributed to the observed differences can not been excluded. On the other hand, the broadening of the endothermic bands could be a result of additional thermal events, such as (*i*) the co-presence of small amounts of amorphous calcium carbonate that converted into the vaterite[33,34] and/or (*ii*) the transition between vaterite structures differently stabilized (or destabilized) by the organic matrix.

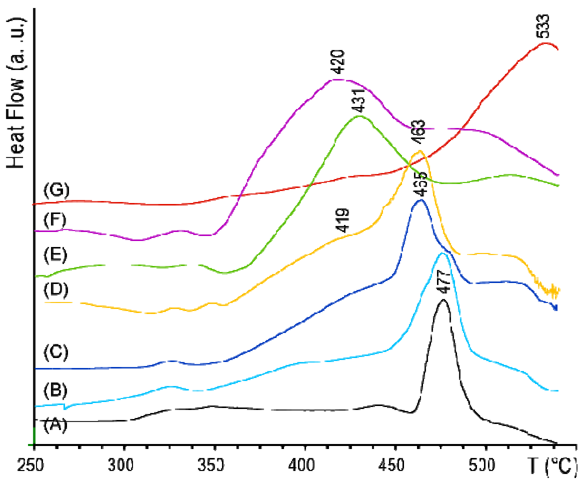

Fig. 4 DSC profiles of: (A) vat1; (B) vat2; (C) vat1-pAsp; (D) vat2-pAsp; (E) *H. momus* spicule; (F) *C. nasus* asteriscus otolith; (G) lackluster pearl.

The enthalpy of the transition from vat1 or vat2 to calcite was about 27 J/g, in agreement with previously published data.[32,35] The transition enthalpies of vat1-Asp and vat2-Asp samples were slightly lower, at about 25 J/g. The broadening of the transition band of the biogenic samples reduced the precision of the estimate of the corresponding transition enthalpy. However, the measured values were found to be similar to other vaterite samples (Table S1). Indeed, the observed broadening of the band pointed to a possibility of more than one thermal transition in a given temperature range.

In conclusion, the obtained results show that vaterite can exist as structures with different degree of disorders and/or as a combination of two or more crystalline structures.[24,25] However, the obtained results cannot exclude the co-presence of ACCs. The differences observed by applying the different techniques (Figs. 2-4) could be related to their varying detection limits for vaterite structures. Despite this, a higher structural variability was observed in the biogenic samples than in the synthetic ones. In the samples of biogenic vaterite, the organic matrix could (de)stabilize metastable phases, which would be consistent with proposed concept of stabilization of metastable mineral phase (e.g. ACCs) by biomineralizing organisms, for functional purposes.[36] The presented data also suggest that the distribution among different crystalline structures is wider in biogenic that in synthetic samples. Moreover, it was observed that the presence of pAsp favored the structural heterogeneity.

Finally, on the basis of the presented experimental data it could be concluded that the certain organisms are able to control the co-existence of different crystalline structures of vaterite, thus enabling optimization for specific functions.

We thank Prof. Feng, Tsinghua University, China, for supplying the Chinese freshwater cultured lackluster pearl. GF and SF thank the CIRC-MSB for the support. We thank Dr. D. M. Smith (RBI) for revising the language.

Notes and references

[a] *Dipartimento di Chimica "G. Ciamician", Alma Mater Studiorum - Universita' di Bologna, via Selmi 2, 40126 Bologna, Italy*
Fax: +39 (0)51 2099456; Tel: +39 (0)51 2099473
E-mail: giuseppe.falini@unibo.it
[b] *Laboratory for Precipitation Processes, Rudjer Boskovic Institute P. O. Box 180, HR–10002 Zagreb, Croatia.*

† Electronic Supplementary Information (ESI) available: [Material and methods, X-ray powder diffraction patterns (Fig. S1). FTIR of vaterite samples before and after the DSC thermal treatment (Fig. S2-S3) and differential scanning calorimeter data (Tab. S1)]. See DOI: 10.1039/b000000x/

1. H. A Lowenstam and S. Weiner (1989) *On biomineralization*. Oxford University Press: New York.
2. S. Mann, (2001) *Biomineralization: Principles and Concepts in Bioinorganic Materials Chemistry*. Oxford University Press, U.K.
3. H.C.W. Skinner, *Mineral. Mag.*, 2005, **69**, 621–641.
4. L. Xiang, Y. Wen, Q. Wang and Y. Jin, *Mat. Chem. Phys.*, 2006, **98**, 236–240.
5. L. Brecevic and D. Kralj, *Croat. Chem. Acta* 2007, **80**, 467-484.
6. D. V. Volodkin, R. von Klitzing and H. Möhwald, *Angew Chem Int Ed Engl.*, 2010, **22**, 9258–9261.
7. X. Yan, J. Li and H. Möhwald, *Adv. Mat.*, 2012, **24**, 2663–2667.
8. W. Ostwald, *Z. Phys. Chem.*, 1897, **22**, 289–330.
9. J. H. Cartwright , A. G. Checa, J. D. Gale, D. Gebauer and C. I. Sainz-Díaz, *Angew Chem Int Ed Engl.,* 2012, **26**, 11960–11970.
10. A. V. Radha and A. Navrotsky, *Rev. Mineral. Geochem.,* 2013, **77**, 73–121.
11. J. Kanakis, P. Malkaj, J. Petroheilos and E. Dalas, *J. Cryst. Growth*, 2001, **223**, 557–564.
12. G. Falini, S. Fermani, S. Vanzo, M. Miletic and G. Zaffino, *Eur. J. Inorg. Chem.*, 2005, **1**, 162–167.
13. U. Wehrmeister, D. E. Jacob, A. L. Soldati, N. Loges, T. Häger and W. Hofmeister, *J. Raman Spectrosc*., 2011, **42**, 926–935.
14. A. P. Ariani, K. J.Wittmann and E. Franco, *Biological Bull.*, 1993, **185**, 393–404.
15. R. Lakshminarayanan, E. O. Chi-Jin, X. J. Loh, R. M. Kini and S. Valiyaveettil, *Biomacromolecules,* 2005, **6**, 1429–1437.
16. L. Qiao, Q.-L. Feng and Z. Li, *Cryst. Growth Des*., 2007, **7**, 275–279.
17. M.-P. Isaure, G. Sarret, E. Harada, Y.-E. Choi, M. A. Marcus, S. C. Fakra, N. Geoffroy, S. Pairis, J. Susini, S. Clemens and A. Manceau, *Geochim. Cosmochim. Acta,* 2010, **74**, 5817–5834.

18. H. A. Lowenstam and D. P. Abbott, *Science,* 1975, **188**, 361–363.
19. D. Kralj and L. Brecevic, *J. Crystal Growth*, 1990, **104**, 793–800.
20. B. Njegic-Dzakula, G. Falini, L. Brecevic, Z. Skoko, D. Kralj *J. Coll. Interface Sci.*, 2010, **343**, 553–563.
21. G. Falini, S. Fermani, M. Gazzano and A. Ripamonti, *Chem. Eur. J.*, 1998, **4**, 1048–1052.
22. E. M. Pouget, P. H. Bomans, J. A. Goos, P. M. Frederik, G. de With and N. A. Sommerdijk, *Science*, 2009, **323**, 1455–1458.
23 H. Colfen and M. Antonietti *Langmuir,* 1998, **14**, 582–589.
24. L. Kabalah-Amitai, B. Mayzel, Y. Kauffman, A. N. Fitch, L. Bloch, P. U. P. A. Gilbert and B. Pokroy, *Science,* 2013, **340**, 454−457.
25. R. Demichelis, P. Raiteri, J. D. Gale and R. Dovesi, *CrystEngComm*, 2012, **14**, 44–47.
26. Y. Politi, T. Arad, E. Klein, S. Weiner and L. Addadi, *Science,* 2004, **306**, 1161–1164.
27. K. M. Poduska, L. Regev, E. Boaretto, L. Addadi, S. Weiner, L. Kronik and S. Curtarolo, *Adv. Mater.,* 2011, **23**, 550–554.
28. M. Suzuki, Y. Dauphin, L. Addadi and S, Weiner, *Crystengcomm*. 2011, **13**, 6780–6786.
29. M. Sato and S. Matsuda, *Zeitschrift fur Kristallographie*, 1969, **129**, 405–455.
30. B. K. Nakamoto, J. Fujita, S. Tanaka and M. Kobayashi, *J. Am. Chem. Soc.*, 1957, **79**, 4904–4908.
31. L. Qiao, Q. L. Feng and Y. Liu, *Mat. Lett.,* 2008, **62**, 1793–1796.
32. G. Wolf and C. Günther, *J. Thermal Anal. Calor.*, 2001, **65**, 687–698.
33. A. V. Radha, T. Z. Forbes, C. E. Killian, P. U. P. A. Gilbert and A. Navrotsky, *Proc. Natl. Acad. Sci. USA,* 2010, **107**, 16438–16443.
34. S. Raz, P. C. Hamilton, F. H. Wilt, S. Weiner and L. Addadi, *Adv. Funct. Mater.*, 2003, **13**, 480–486.
35. J. Peric, M. Vucak, R. Krstulovic, L. Brecevic and D. Kralj, *Thermochim. Acta,* 1996, **277**, 175–186.
36. L. Addadi, S. Raz and S. Weiner, *Adv. Mater.*, 2003, **15**, 959–970.